Supporting Information

Lo et al. 10.1073/pnas.1301664110

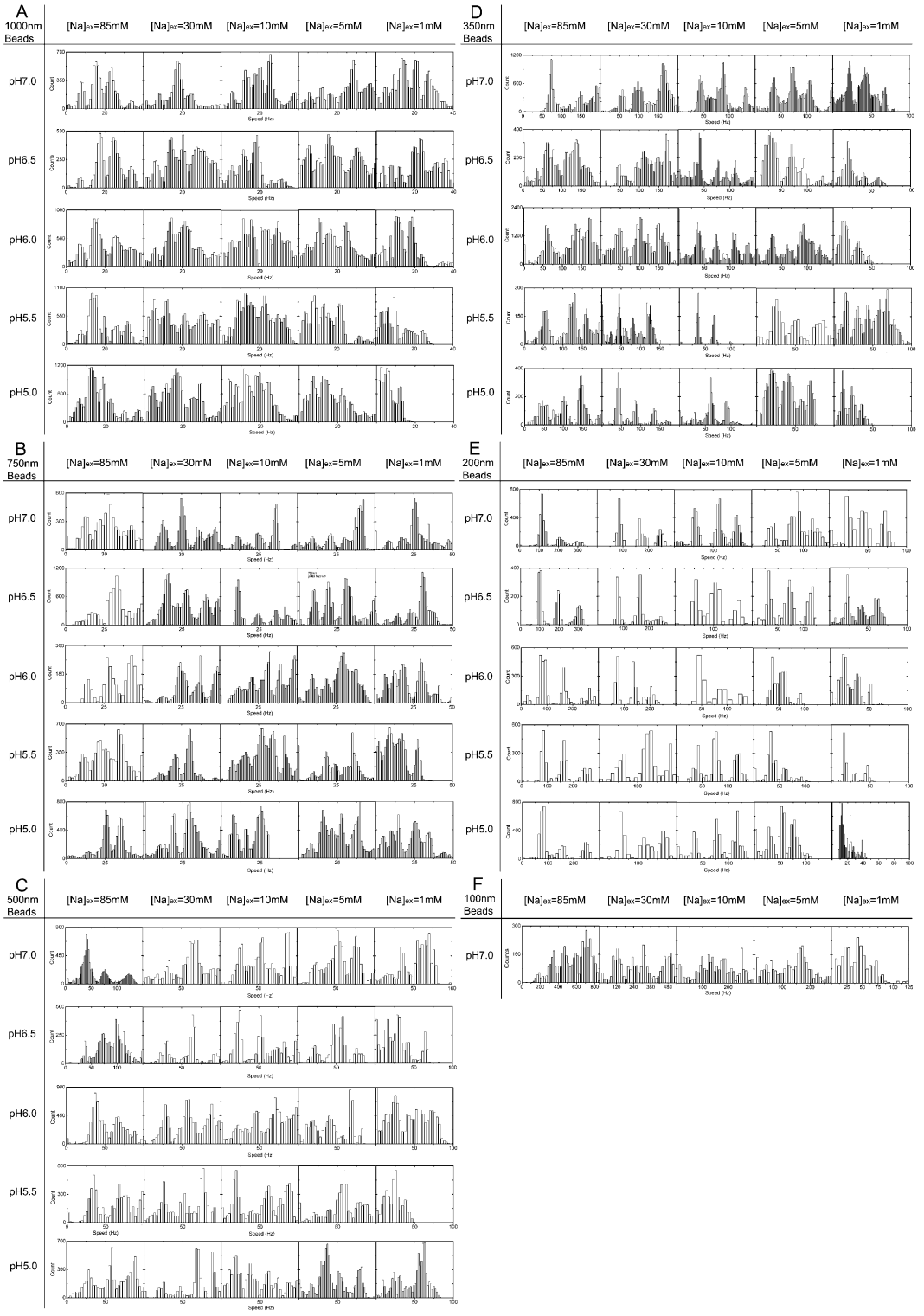

Fig. S1. Histogram of all speed measurements in different energetic conditions. (*A*) 1,000-nm beads; (*B*) 750-nm beads; (*C*) 500-nm beads; (*D*) 350-nm beads; (*E*) 200-nm beads; (*F*) 100-nm beads.

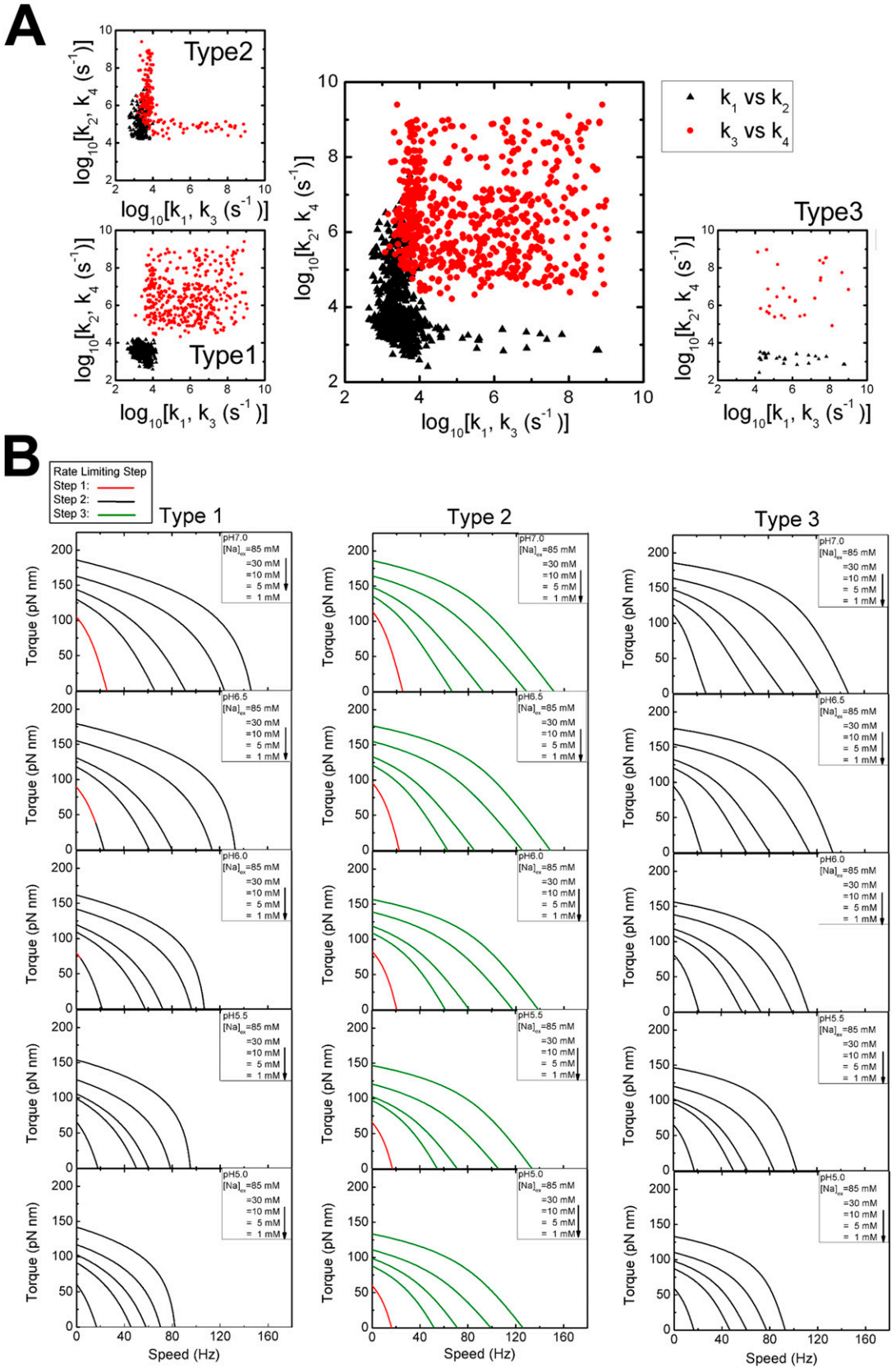

Fig. S2. Exploration of the pattern of rate constants and rate-limiting steps. (*A*) The set of possible solutions is projected onto two-dimensional plots of k_1 vs. k_2 (*Center*, black) and k_3 vs. k_4 (*Center*, red). A total of 65.5% of solutions fall into the category labeled "type 1" defined as k_1, $k_2 < 10^{4.2}$ s^{-1}, with k_3 and k_4 typically faster (*Inset*, *Lower Left*). Two alternative possibilities are also illustrated. For "type 2" solutions ($k_2 > 10^{4.2}$ s^{-1}, 30.4% of the total), k_1 remains slow but k_3 replaces k_2 as the limiting transition rate at $[Na^+] > 1$ mM (*Inset*, *Upper Left*). We also found "type 3" solutions ($k_1 > 10^{4.2}$ s^{-1}, 4.1% of the total) for which all

Legend continued on following page

of $k_{1,3,4}$ are fast and k_2 is always rate limiting (*Inset*, *Lower Right*). (*B*) Simulated torque–speed curves from the four-state model, illustrating the rate-limiting step for each type. The parameter set with the lowest cost function is shown for each type of solution. The colors of the torque–speed curves indicate the transition with the slowest forward rate at that point (red, black, and green for steps 1, 2, and 3, respectively).

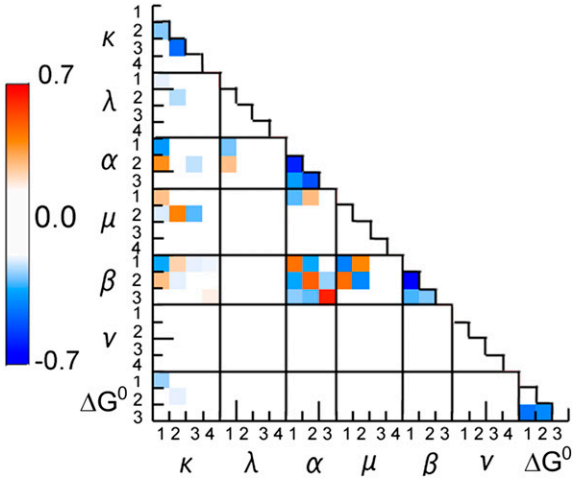

Fig. S3. Cross correlations between all pairs of parameters in the 830 parameter sets. Red shows positive correlations and blue negative correlations. Negative correlations between k_i support the identification above of alternative types of solution (Fig. S2): If one transition is rate limiting, another is less likely to be. Strong positive correlations between α_i and β_i indicate a powerstroke mechanism: Charge movement driven by V_m and rotation occur together in a single step. This was previously observed to be necessary to model the characteristic concave-down torque–speed curve of fully energized wild-type H^+ motors. Negative correlations between α_i and α_j, β_i and β_j, ΔG_i^0 and ΔG_j^0, $j \neq i$, are a consequence of the constraints $\Sigma(\alpha_i) = \Sigma(\beta_i) = 1$ and $\sum(\Delta G_i^0) = 0$. Negative correlations between α_i and β_j follow from positive correlations between α_i and β_i and negative correlations between α_i and α_j and β_i and β_j. A powerstroke mechanism is further supported by negative correlations between α_i, β_i, and k_i: The powerstroke must be one of the slower, rate-limiting transitions. Correlations between μ_i and α_i (−ve), μ_i and β_i (−ve), and μ_i and k_i (+ve) indicate that the powerstroke, associated with high α, β and low k, is likely to have a low value of μ: External resisting torque speeds up the reverse powerstroke rather than slowing the forward powerstroke. This allows the motor to run at high speeds even at high torque, maximizing mechanical power output. Microscopically, it predicts that the angle of the transition state is close to that of the previous state (1), which is another signature of a "powerstroke": The driving electrochemical transition occurs without large-scale movement of the motor as a whole, allowing forced rather than slow diffusive motion of the motor.

1. Kolomeisky AB, Fisher ME (2007) Molecular motors: A theorist's perspective. *Annu Rev Phys Chem* 58:675–695.

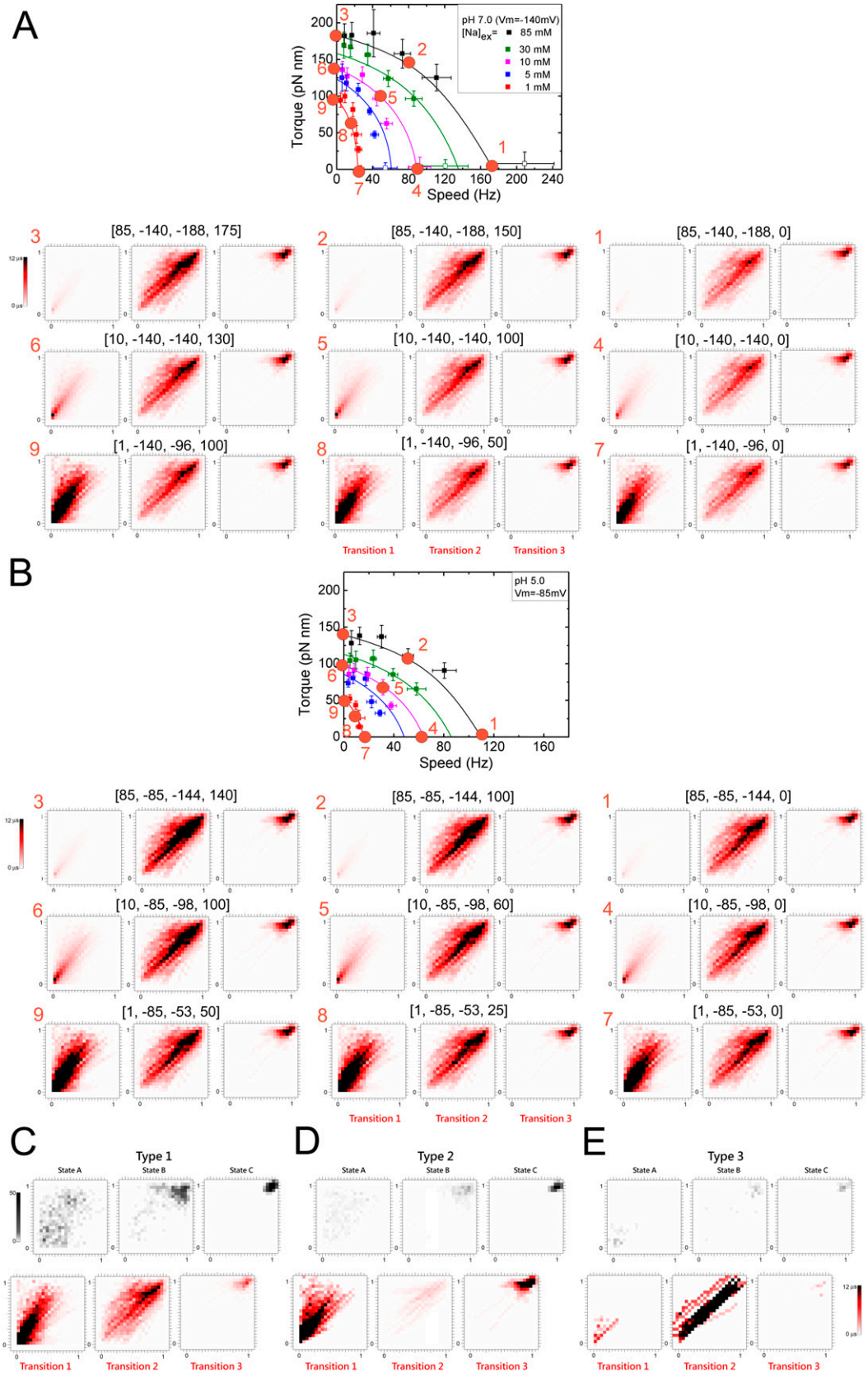

Fig. S4. Distributions of transitions in the 830 parameter sets found to be consistent with data, calculated under different conditions. Each transition in each parameter set is represented by a line with weight equal to the forward transition time. This emphasizes the transitions that are rate limiting. (*A* and *B*) Each section reproduces a panel from Fig. 3, labeling the conditions for which transition distributions are illustrated. Conditions are also indicated in brackets as [external sodium concentration [Na^+], membrane voltage (V_m), sodium-motive force (SMF), and torque]. (*A* and *B*) Distributions for (*A*) $V_m = -140$ mV and (*B*)

Legend continued on following page

V_m = −85 mV. Powerstrokes in step 2, ion transit, are always rate limiting. Powerstrokes in step 1 are rate limiting at low [Na^+]. (*C–E*) Distributions of states (*Upper*) and transitions (*Lower*) for [Na^+] = 1 mM, V_m = −140 mV, torque = 50 pN nm, as in Fig. 5*C*, for each of the subtypes of solutions identified in Fig. S2. (*C*) "Type 1" solutions (k_1 and $k_2 < 10^{4.2}$ s^{-1}, 65.5% of the total), where k_1 and k_2 are both slow and ion transition is the rate-limiting step except at 1 mM [Na^+] (Fig. S2*A*, *Lower Left Inset*). (*D*) "Type 2" solutions ($k_2 > 10^{4.2}$ s^{-1}, 30.4% of the total), where k_1 remains slow but k_3 replaces k_2 as the limiting transition rate at [Na^+] > 1 mM (Fig. S2*A*, *Upper Left Inset*). Note that transition 3, ion release into the cytoplasm, is not a powerstroke in these solutions, despite being rate limiting. (*E*) "Type 3" solutions ($k_1 > 10^{4.2}$ s^{-1}, 4.1% of the total), for which all of $k_{1,3,4}$ are fast and k_2 is always rate limiting (Fig. S2*A*, *Lower Right Inset*). Transition 2, ion transit, is the rate-limiting powerstroke in these solutions.

Table S1. Sodium-motive force

	$[Na^+]_{ex}$					
pH	85 mM	30 mM	10 mM	5 mM	1 mM	
7	*−140*	*−136*	*−141*	*−141*	*−143*	V_m, mV
	13.4	*10.8*	*9.9*	*8.7*	*5.5*	$[Na]_{in}$, mM
	−48	−26	0	14	44	$\Delta\mu/q$, mV
	−188	**−162**	**−141**	**−127**	**−99**	**SMF, mV**
6.5	*−126*	*−125*	*−126*	*−123*	−123	V_m, mV
	9.9	*9.2*	*9.1*	*6.9*	4.6	$[Na]_{in}$, mM
	−56	−30	−2	9	40	$\Delta\mu/q$, mV
	−182	**−155**	**−128**	**−114**	**−83**	**SMF, mV**
6	*−107*	*−108*	*−108*	*−106*	−108	V_m, mV
	9.6	*8.1*	*7.0*	*5.1*	3.9	$[Na]_{in}$, mM
	−56	−34	−9	1	35	$\Delta\mu/q$, mV
	−163	**−142**	**−117**	**−105**	**−73**	**SMF, mV**
5.5	*−96*	*−92*	*−94*	*−97*	−93	V_m, mV
	8.4	*8.4*	*7.2*	*5.3*	3.7	$[Na]_{in}$, mM
	−60	−33	−9	2	34	$\Delta\mu/q$, mV
	−156	**−125**	**−103**	**−95**	**−59**	**SMF, mV**
5	*−84*	*−83*	*−87*	*−86*	*−86*	V_m, mV
	8.8	*8.5*	*6.1*	*4.6*	*3.4*	$[Na]_{in}$, mM
	−59	−33	−13	−2	32	$\Delta\mu/q$, mV
	−143	**−116**	**−100**	**−88**	**−54**	**SMF, mV**

Shown are the individual components (V_m and $\Delta\mu/q$) and the total SMF at the values of pH and external sodium concentration under which we measured torque–speed curves (Fig. 3). Data are taken from refs. 1 and 2: V_m and $[Na]_{in}$ (numbers in italics) are averages of measurements on 50 single cells, which are used to calculate the corresponding values of $\Delta\mu/q$ and SMF (boldface). SDs of V_m and $\Delta\mu/q$ measurements are typically 13 mV and 5 mV, respectively.

1. Lo CJ, Leake MC, Berry RM (2006) Fluorescence measurement of intracellular sodium concentration in single *Escherichia coli* cells. *Biophys J* 90(1):357–365.
2. Lo CJ, Leake MC, Pilizota T, Berry RM (2007) Nonequivalence of membrane voltage and ion-gradient as driving forces for the bacterial flagellar motor at low load. *Biophys J* 93(1): 294–302.

Dataset S1. Excel file of 830 parameter sets found

Dataset S1